Materials Research Express

Bismuth Ferrite thin film as an efficient electrode for photocatalytic degradation of Methylene Blue Dye

To cite this article before publication: Pratik Vijaysinh Mane *et al* 2018 *Mater. Res. Express* in press https://doi.org/10.1088/2053-1591/aaf096

Bismuth Ferrite thin film as an efficient electrode for photocatalytic degradation of Methylene Blue Dye

P. V. Mane[1], N. B. Shinde[1,#], I. M. Mulla[1,2], R. R. Koli[1], A. R. Shelke[1], M. M. Karanjkar[2], S. R. Gosavi[3*], and N. G. Deshpande[1*]

[1]q-SPIN Tech and Nanomaterials Laboratory, Department of Physics, Shivaji University, Kolhapur-416004 (M.S.) India.

[2]Department of Physics, Vivekanand College, Kolhapur (M.S.) India.

[3]Material Research Laboratory, C. H. C. Arts, S. G. P. Commerce and B. B. J. P. Science College, Taloda, Dist. Nandurbar-425413, (M. S.), India.

*corresponding author: srgosavi.taloda@gmail.com (SRG) nicedeshpande@yahoo.co.in (NGD)

[#]Current Address: Department of Physics, SRM University, Chennai, India

ABSTRACT

The Bismuth Ferrite [$BiFeO_3$-(BFO)] thin film, as a visible-light-driven photocatalytic electrode, is synthesized using the simple spray pyrolysis method. BFO thin films prepared at different precursor concentrations of 4 mM, 6 mM, 8 mM and 10 mM are utilized to degrade organic dyes such as Methylene blue (MB), Congo red (CR), Ponceau-S (PS) at different light irradiation times. Single-phase and polycrystalline nature with rhombohedral crystal structure are observed for all the BFO samples. BFO is seen to have hydrophilic nature for the films deposited at 6, 8 and 10 mM, which transits to the hydrophobic nature for films deposited at lower concentration of 4 mM. The optical study reveals light absorption in the visible-region of the electromagnetic spectrum for all the BFO samples indicating the use of BFO as photoelectrode in visible-region. BFO samples showed photocatalytic degradation activity with its reusability for the studied dyes i.e., MB, CR, and PS. Significantly, higher efficiency of MB dye degradation was noted. Moreover, after MB dye degradation, the physical properties of BFO film are again studied, which indicated good stability for BFO sample prepared at 10 mM precursor concentration.

Keywords: *Bismuth Ferrite; Methylene blue; Photocatalysis; Spray pyrolysis method*

1. Introduction

The increase in textile industries results in the large production of daily waste (byproducts), which when exposed to the environment, causes several issues [1-3] concern to air and water pollutions. In particular, the organic toxic pollutants such as azo dyes from the industries raise much more concern for ecological systems [4-11]. Larger use of these dyes is because of their high solubility and color variety. On contrary, these dyes even at low concentration stop photosynthesis process and due to toxicity, they are dangerous to aquatic lives. In the last few years, extensive efforts have been carried out for the development of different technologies to eradicate the organic and inorganic pollutants that are harmful to the ecological systems. Among all, photocatalysis is one of the upcoming technologies, which is safe, effective and can be reusable. Usually, semiconductors with suitable band-gap such as TiO_2, WO_3, ZnO, CdS, ZnS, etc. are used as photoelectrodes for photocatalytic degradation. Among all, TiO_2 [12-16] is most often used as an efficient photocatalytic electrode. But TiO_2 has some practical limitation concerning to its large band-gap i.e., it absorbs only UV light, which has a very little contribution (i.e., 5%) in the solar spectrum. On the other hand, CdS that absorbs the light in visible-region is also studied by several researchers [17-20]. However, CdS has issues concern to its own degradation with the dyes. Apart from this 'Cd' is toxic in nature. This may limit its reusability for longer runs. So a search for a proper alternative that replaces all the above materials and their concerned issues is necessary.

Accordingly, we have synthesized Bismuth Ferrite [$BiFeO_3$-(BFO)], which is a potential visible-light-driven photocatalyst for the degradation of organic dyes [21-23]. BFO has narrow band-gap (~ 2.2 eV) and has excellent chemical stability [24]. Wang et al. [25] prepared BFO nanoparticles by using a sol-gel method and found that the morphology and surface-area had a remarkable influence on photocatalytic activity under visible-light. Annapu Reddy et al. [26] synthesized nanocrystalline BFO by spray pyrolysis method. They have studied optical, electrical and structural properties of spray deposited BFO films. The absorption spectra of the film show large band-gap for small grain size film. Deng et al. [27] also prepared single phase BFO nanoparticles, which showed a highly efficient photocatalytic activity of water decomposition under the simulated solar light. Soltani et al. [28] studied BFO for degradation of RB5 dye kinetically. Chen et al. [29] prepared BFO films by pulsed laser deposition on $Pt/TiO_2/SiO_2/Si$ substrates and studied them as photoelectrodes for water splitting. Ramesh and his group [25, 30, 31] have reported on the bulk photovoltaic properties of BFO where photocurrent can flow in a uniform material without the need to form an interface (p–n junction). Although research work related to BFO is carried out; but

comprehensive work related to photocatalytic degradation and reusability of BFO electrode is rarely found. Moreover, results on the percentage degradation of different dyes and the selectivity using BFO as a photocatalyst is rarely found in the literature. So that in this work we have synthesized BFO thin films via simple spray pyrolysis method and applied them for degradation of Methylene Blue (MB), Congo Red (CR), and Ponceau-S (PS) dyes. Usually, these dyes are considered as representative dyes of the textile wastewaters. The various parameters are examined to find out the optimum condition to remove colour and impurities from the water. Eventually, its reusability is studied and discussed herein.

2. Experimental details

2.1 Materials

All chemicals used in the present work were AR grade obtained from Merck Specialties Private Ltd., Mumbai. For the thin film deposition of $BiFeO_3$, Bismuth nitrate [$Bi(NO_3)_3.5H_2O$], Ferric nitrate [$Fe(NO_3)_3.9H_2O$], an aqueous HNO_3 solution were utilized as precursor solutions. For photocatalytic degradation study, Methylene blue (Methylthioninium chloride), Ponceau-S [3-hydroxy-4-(2-sulfo-4-[4-Sulfo phenyl azo] phenyl azo)-2,7-naphthalene disulfonic acid sodium salt] and Congo Red [disodium 4-amino-3-[4-[4-(1-amino-4-sulfonato naphthalen-2-yl) diazenylphenyl] phenyl] diazenyl naphthalene -1-sulfonate] were employed as model dyes. An aqueous solution of each dye in distilled water is served as a wastewater pollutant during photodegradation experiment.

2.2 Preparation of Precursor Solution

For the deposition of BFO thin films, 4 mM $Bi(NO_3)_3 \cdot 5H_2O$ and $Fe(NO_3)_3 \cdot 9H_2O$ were dissolved in 20 ml of the initially prepared aqueous HNO_3 solution in separate beakers. Further, they were mixed in a single beaker and constantly stirred to achieve uniformity. Overall 40 ml of 4 mM (Bismuth nitrate + Ferric nitrate along with aqueous HNO_3) solution is taken in a beaker, which forms the final spraying solution. A similar procedure is applied to prepare the final spraying solution with different concentrations 6 mM, 8 mM, 10 mM and used for the synthesis of BFO thin films using a spray pyrolysis method. The films were deposited onto the ultra cleaned glass substrate of 2.5×7.5 cm^2 size. The BFO films were deposited at the different concentrations such as 4 mM, 6 mM, 8 mM and 10 mM. Accordingly, they are coded as BFO_04, BFO_06, BFO_08, and BFO_10, respectively and used throughout in the manuscript. Further, all these BFO samples were annealed at 350^{o}C for 3 hours to obtain proper phase and crystallinity.

2.3 Characterizations and Photocatalytic activity study

The BFO thin films were characterized for structural, morphological, optical and surface properties. Thickness of the thin films was measured using surface profiler (XP stylus profiler instruments). Structural properties were studied using X-ray diffractometer provided by Bruker D2 phaser. Morphological studies were carried out using the scanning electron microscopy (SEM) provided by JEOL JSM-6360. Optical properties were studied using a UV-VIS spectrophotometer provided by JASCO V-630 UV-VIS spectrophotometer. The surface wettability was measured using RAME-HART contact angle goniometer. Further, a simple experimental set-up was utilized for the photocatalytic degradation of MB, CR, and PS dyes. MB, CR, and PS are the widely used dyes in industries that are studied here as representative dye pollutants to evaluate the photocatalytic activity of BFO thin films. The photocatalytic activity was investigated under visible-light irradiation with PHILIPS 160 W Hg lamp at room temperature (RT). The BFO thin films were placed in a beaker containing 60 ml of 1 ppm aqueous solutions of MB, PS and CR dyes. During the photocatalytic study, it is found that the absorbance peaks of MB, PS, and CR revealed at 651 nm, 525 nm and 490 nm, respectively and they are directly proportional to the concentrations. Hence, the efficiency of the degradation process was monitored through the absorption at the maximum absorption peak around λ_{max} = 651 nm for MB, 525 nm for PS and 490 nm for CR as a function of irradiation time (1 to 10 h at the interval of 1 h), using a JASCO V-630 UV-VIS spectrophotometer. The degradation of MB, PS, and CR can be calculated by the following formula,

$$\% \text{ Degradation } = \frac{C_o - C_t}{C_o} \times 100 \quad (1)$$

where 'C_o' represents the initial concentration, 'C_t' represents the concentration after time 't' of treatment with MB, PS, and CR at the characteristic absorbance wavelength.

3. Result and Discussions

3.1. Structural studies

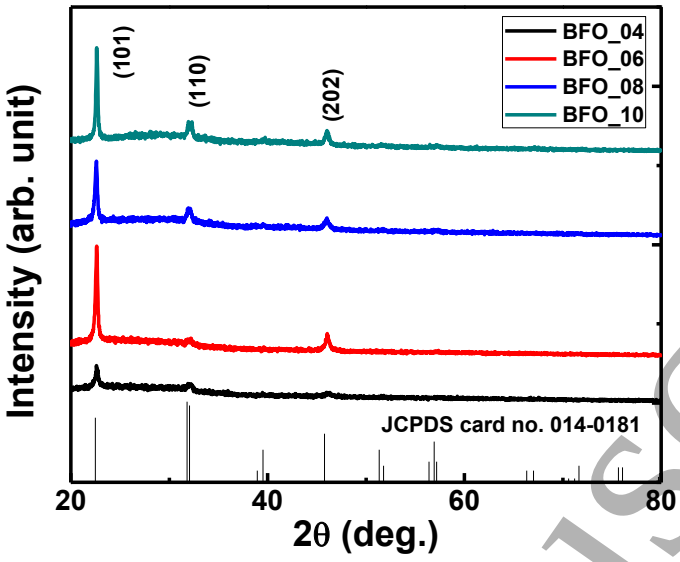

Fig. 1 XRD patterns of as-deposited BFO thin films deposited at various concentrations of precursor solution i.e., 4mM (BFO_04), 6 mM (BFO_06), 8 mM (BFO_08), and 10 mM (BFO_10).

Figure 1 shows the XRD patterns of as-deposited BFO thin films i.e., BFO_04, BFO_06, BFO_08, and BFO_10. It is observed that all the samples exhibited single-phase with polycrystalline nature. A comparison to the JCPDS card No. 014-0181 indicated that all the XRD data belong to the rhombohedral crystalline structure. The films are found to be highly oriented along (101) plane indicating the preferential growth of the BFO along this particular direction. The average crystallite size using standard Sherrer's formula [32-33] was calculated and found to be 15.25 nm, 12.16 nm, 9.46 nm, and 7.74 nm for BFO_04, BFO_06, BFO_08, and BFO_10, respectively. It is seen that the crystallite size decreases with an increase in the precursor concentration. Further, an uneven change in the intensity with change in the precursor concentration is noted that indicates there is no proper relation between the change in precursor concentration and the crystallinity.

3.2. Surface Morphology and Wettability study

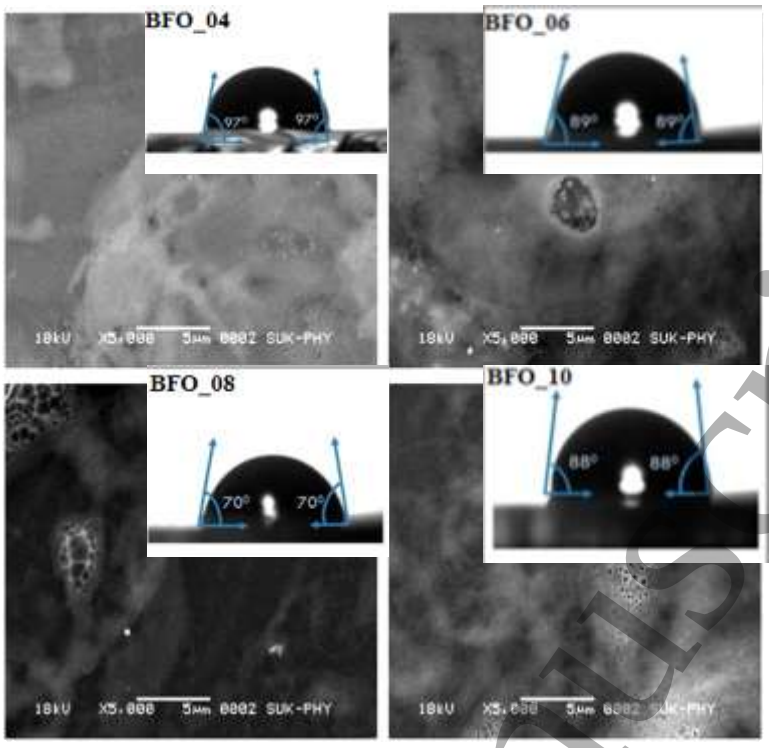

Fig. 2 SEM images of BFO thin films deposited at different precursor concentrations i.e., BFO_04, BFO_06, BFO_08 and BFO_10 and the inset shows corresponding water contact angle images of BFO thin films.

Fig. 2 shows the surface morphology of the BFO samples deposited at various concentrations. Although the surface is not properly resolved, it still indicates a granular morphology with very smaller grains that are compact together. Moreover, the BFO films deposited at higher concentrations indicated presence of voids over the surface. Such kind of morphology is often evolved for spray deposited samples [34, 35]. Furthermore the surface wettability study of all BFO thin films is carried out by measuring the water contact angle, which is shown in the inset of Fig. 2. It is observed that the water contact angle for the BFO_06, BFO_08, and BFO_10 is 89^0, 70^0 and 88^0, respectively, indicating the hydrophilic nature of the surface. On the other hand, at lower concentration i.e., for BFO_04, the water contact angle was found to be 97^0 (hydrophobic nature of the surface). This indicates that there is a transition from the hydrophilic nature of the BFO films deposited at 6, 8 and 10 mM to the hydrophobic nature of the film deposited at low concentration of 4 mM. Such a high value of the water contact angle comes into account due to the reduced surface energy and better compact surface morphology as compared with other BFO films [36-39]. This is equally corroborated by the surface morphology as seen in the Fig. 2. It is observed from the figure that all samples exhibit compact surface morphology. As concentration increases,

some voids are observed, which helps in decreasing the contact angle. Therefore, samples BFO_06, BFO_08 and BFO_10 are expected to intercalate more dye as compared to the sample BFO_04, which will thereby directly influence the dye degradation efficiency.

3.3. Optical Study

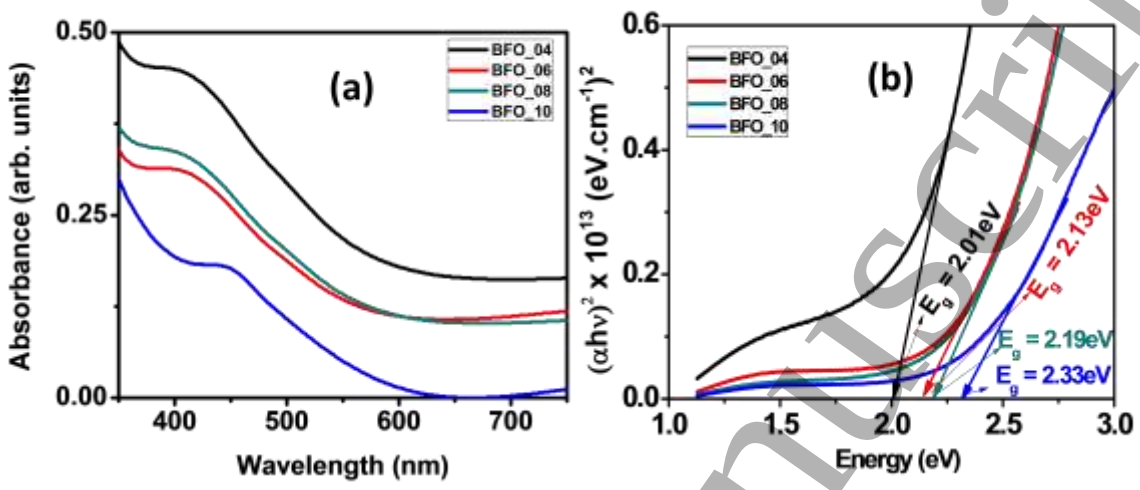

Fig. 3 (a) Plot of absorbance versus wavelength for BFO thin films deposited at various concentrations i.e., BFO_04, BFO_06, BFO_08, and BFO_10. (b) The corresponding plot of $(\alpha h\nu)^2$ versus energy for BFO films deposited at different concentrations i.e., BFO_04, BFO_06, BFO_08, and BFO_10.

Fig. 3 (a) shows optical absorbance spectra of as-deposited BFO films deposited at different precursor concentrations. The absorbance is higher at the lower wavelength side and it gradually decreases and becomes flat towards higher wavelength side. The absorbance of BFO in a visible region is due to the electron-excitation from oxygen *2p* to iron *3d* level. The absorbance for BFO_04 sample shows higher absorbance as compared to BFO_06, BFO_08, and BFO_10 samples. This again can be equally substantiated with the compact nature of the BFO_04 film. Further, using the absorbance spectra, the band-gap (E_g) values are calculated by plotting $(\alpha h\nu)^2$ versus energy and extrapolating the linear portion to get the intercepts along the energy axis [see Fig. 3 (b)]. The band-gap energies of BFO_04, BFO_06, BFO_08 and BFO_10 thin films are found to be 2.01 eV, 2.11 eV, 2.19 eV, and 2.33 eV, respectively. The E_g value increases with the increase in the precursor concentrations. All the E_g values were found to be in the visible region, which is essential to achieve the photocatalytic activities in the visible region and utilize the large energy spectrum within the visible region.

4.1 Photocatalytic Degradation study

4.1.1 Mechanism of photodegradation

Among all recent oxidation methods, heterogeneous photocatalysis has proven to be an efficient tool for degrading organic contaminants. In heterogeneous photocatalysis, photoreaction is accelerated in presence of MB, PS and CR dyes, respectively. When BFO is irradiated with the visible-light, an electron e^- from valence band (VB) gets excited to the conduction band (CB) of BFO film. This leaves behind the photogenerated hole (h^+) in VB of BFO film. This charge separation is maintained and electron e^- as well as hole h^+ get migrated to the surface of BFO where they participate in redox reactions. The h^+ in VB may react with surface-bound OH^- to produce hydroxyl radical and electron e^- in CB are taken by oxygen to generate superoxide radical anion (O_2^-). Further, OH^- can be generated in the number of ways, whose oxidation involves following steps [40, 41]-

Absorption of a photon by BFO

$$BFO + h\nu \rightarrow e_{CB}^- + h_{VB}^+ \quad (2)$$

Oxygen reduction

$$(O_2)_{ads} + e_{CB}^- \rightarrow O_2^- \quad (3)$$

Formation of OH^-

$$(H_2O \rightarrow H^+ + OH^-)_{ads} + h_{VB}^+ \rightarrow H^+ + OH^- \quad (4)$$

Neutralization of O_2^- by photons

$$O_2^- + H^+ \rightarrow HO_2 \quad (5)$$

Rapid decomposition of HO_2 to become $OH^\cdot$

$$2HO_2 + e_{CB}^- \rightarrow OH^- + OH^\cdot + O_2 \quad (6)$$

Final products

$$Dye(MB/PS/CR) + OH^\cdot \rightarrow \text{Products}(CO_2 + H_2O + NH_4^+ + SO_4^{2-} + Cl^-) \quad (7)$$

4.1.2 Photocatalytic studies

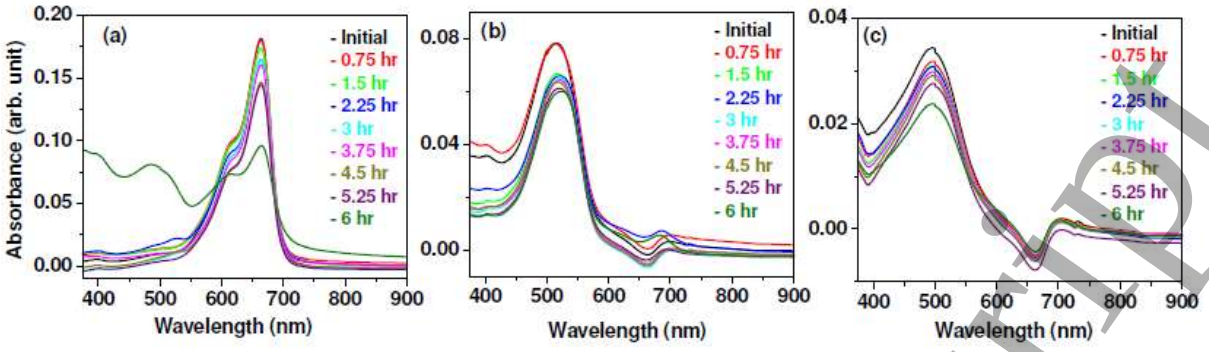

Fig. 4 UV–visible absorption spectra of (a) Methylene blue (MB), (b) Ponceau-S (PS), and (c) Congo red (CR) dyes at different irradiation times with BFO thin film (representative data of BFO_06)

Fig. 4 (a-c) shows the absorbance spectra in presence of MB, PS and CR dye, respectively at different irradiation time i.e., 0 to 6 hr at an interval of 0.75 hr. It contains three strong absorption peaks at 651 nm, 525 nm and 490 nm corresponding to the MB, PS, and CR, respectively. This suggests that all the dyes absorb the light in visible-region. The peak at 525 nm for PS is due to naphthalene component of the benzene ring. The peak at 651 nm in MB stands for chromophore structure and CR showed the maximum absorbance at 490 nm. A significant decrease in the absorbance for various dyes after visible-light irradiation suggests the decolourization [42] i.e., a reduction in the concentration of the dye with time. Absorption peaks are decreased in intensity with increasing irradiation time. The rapid disappearance of the characteristic peak suggests that the structure responsible for dye colour is breaking down. The new intermediates formed during degradation time in visible-region are related to sulphate and nitrate groups [43].

4.2 Optimization of dye

Fig. 5 shows the degradation efficiency with respect to the irradiation time. In the case of PS dye, the degradation increases initially and then it degrades at a constant rate. It shows maximum degradation up to 22%. Further, in the case of CR, a smooth increase in the degradation efficiency is found. CR degrades to near about 30%. For MB dye degradation, it is found that a steady increase of dye degradation efficiency with the irradiation time of 5.25 hr is observed, which accelerates rapidly thereafter. This is because of the fast interaction between the dye and the photocatalyst, which helps for MB to degrade about 48%. Cleavage of (-S-) bond in MB and (-N=N-) bond in CR and PS are responsible for the decolouration. It

is noteworthy that, in a particular irradiation time, the oxidation of thiazine group (-S-) in MB by a positive hole or hydroxyl radical is much easier than oxidation of azo (-N=N-) [44]. So we optimized MB dye for further detailed degradation studies.

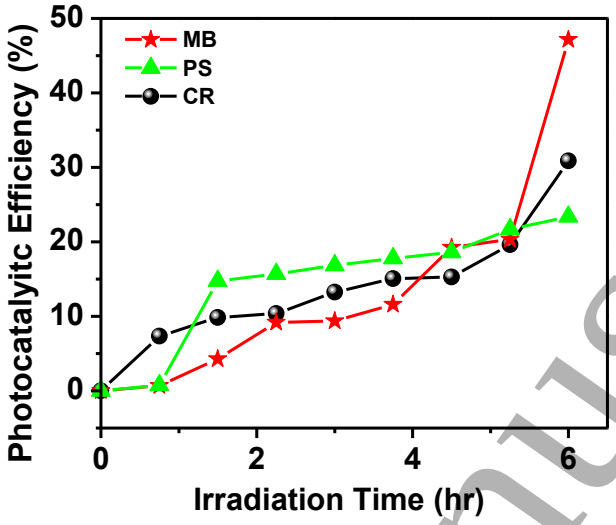

Fig. 5 Percentage degradation of different dyes (MB, PS and Cr) with irradiation time

4.3 Degradation studies of MB dye for BFO deposited at different precursor concentrations

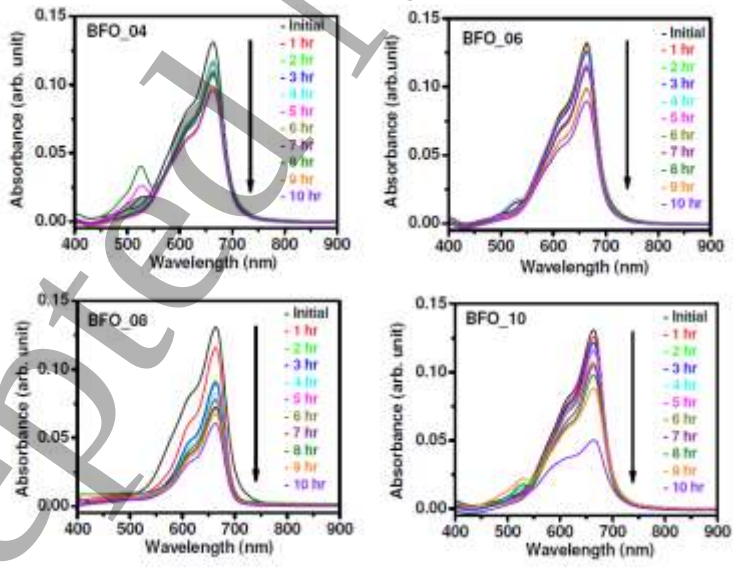

Fig. 6 Absorbance spectra for MB dye degradation with visible-light irradiation in presence of BFO thin films deposited at different precursor concentrations

Fig. 6 shows absorbance for MB dye degradation studies in the presence of BFO thin films deposited at different precursor concentration obtained at different irradiation times (10 hours with an interval of 1 hour). The absorbance peaks at about 650 nm were observed, which is a characteristic peak of the MB dye. As time passes absorbance decreases due to degradation of MB dye in presence of BFO photocatalyst. Decolouration of MB occurs from blue to colourless indicating the breaking down of the larger molecules into smaller molecules. Interestingly, the BFO_10 sample shows a rapid degradation initially and later saturates with irradiation time.

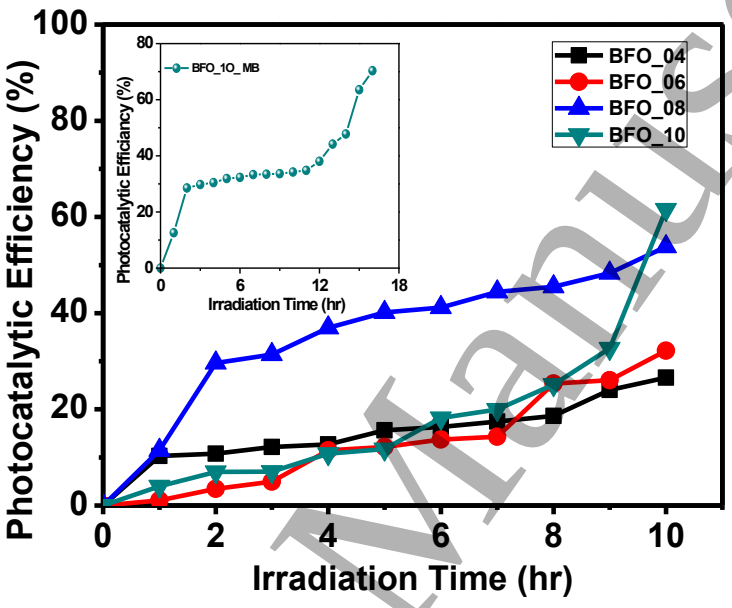

Fig. 7 Percentage degradation of MB for BFO catalyst with different concentrations for 10 hours and the inset shows the reuse of BFO_10 sample showing percentage degradation with the increased irradiation time of 15 hours.

Fig. 7 shows the percentage of MB dye that was degraded by BFO photocatalysts deposited at various precursor concentrations. BFO sample with 4 mM, 6 mM, and 8 mM degrades MB dye up to 25%, 30%, 57%, respectively, while BFO sample with 10 mM concentration degrades MB to a greater percentage of about 64%. This shows that MB dye is efficiently degraded by the BFO_10 sample. This is because BFO_10 sample has high crystallinity, and relatively suitable morphology, which helps in increasing the photocatalytic efficiency [45]. Importantly, the degradation with this sample i.e., BFO_10 still shows some increasing trends. Therefore, we again studied the degradation of the MB dye for this particular sample BFO_10 for up to 15 hours. This sample shows an increase in the percentage of degradation

i.e., it increases from 64% to 74% as irradiation time increases. This result also proves that BFO_10 sample is reusable as it still shows some increasing trend (see inset of fig. 7).

5. Analysis of BFO photoelectrode after dye degradation studies

5.1 Structural studies

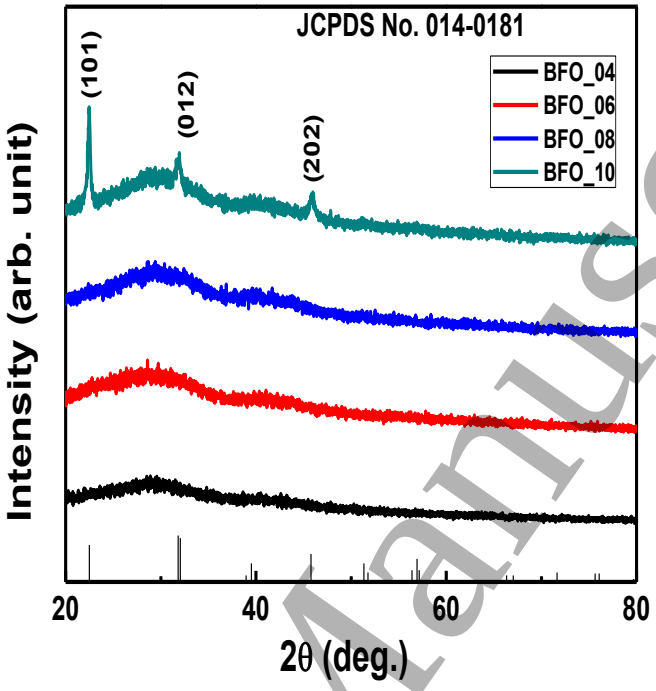

Fig. 8 XRD pattern of BFO photoelectrodes deposited at different precursor concentrations after their utility in dye degradation.

Fig. 8 shows XRD patterns of BFO thin films (deposited at various precursor concentrations) taken after their use in degradation of the MB dye. It clearly shows that the intensity of the peaks for BFO_10 sample is decreased slightly, while samples with BFO_04, BFO_06, and BFO_08 lose their crystallinity after degradation of MB dye. This is due to the fact that; the intermediate ions like SO_4^{--}, NO_3^-, which were formed during catalysis, get adsorbed on the surface of the BFO and suppresses the crystallinity of the BFO samples. But sample with 10 mM concentration has enough stability to hold its crystalline form after degradation. This result shows that BFO sample with 10 mM concentration is reusable for further degradation study as it maintains its crystallinity property intact with repeated utility.

5.2 Optical study

Fig. 9 (a) shows optical absorbance spectra of BFO samples deposited at different precursor concentrations and taken after the MB dye degradation process. It is noted that after the

degradation process, the absorbance for BFO photoelectrodes still lies in the visible region. However, the absorbance value decreases from BFO_04 to BFO_10 sample, which was not observed in the case of BFO samples before the degradation process. This continuous reduction in the absorbance value and change in the trend of the absorbance (with respect to precursor concentration) before and after degradation indicates the possible influence of the absorbing dye (here MB) on the BFO electrode, which is in conjunction with XRD studies (Fig. 8). These impurity ions get intercalated with the BFO and peel of top surface of it so that absorbance changes.

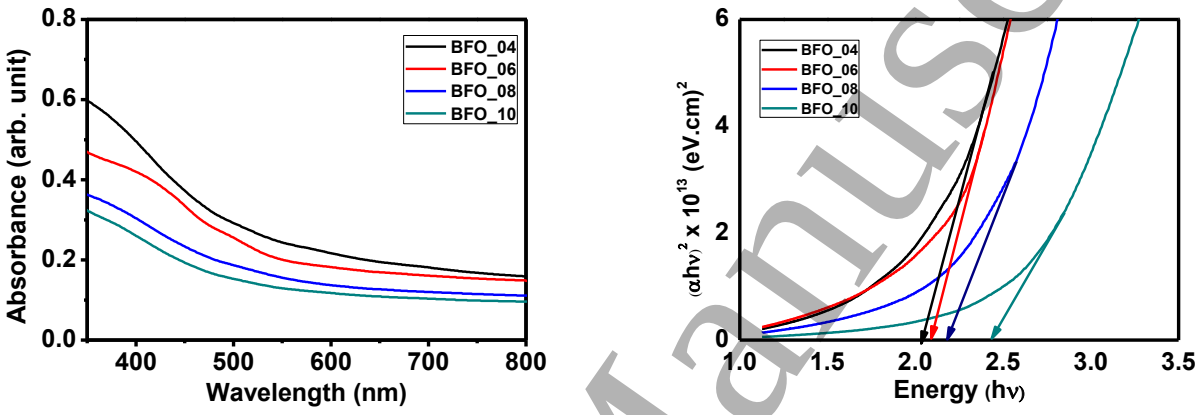

Fig. 9 (a) Optical absorbance spectra of BFO thin films at various concentrations after degradation process and (b) plot of $(\alpha h\nu)^2$ versus (hν) for BFO thin films at various concentrations after degradation process.

Furthermore, Fig. 9 (b) shows the plot of band-gap energy indicating that the band-gap decreases after the degradation process. The band-gap energies after degradation are reduced because the thickness of the samples was found to get decreased after degradation. Although this might be not the only reason for changes observed in the band-gap values, there are several other possibilities like adsorption of dye molecules, etc. But further analysis is needed to confirm for such phenomena's.

This indicates that after the degradation process there is a drastic change in the material properties and hence, this limits the reusability of the electrode. However, 10 mM BFO sample have shown to remain intact with most of their physical properties indicating that BFO_10 photoelectrode is stable and can be re-utilized several times in the degradation process. All the studied properties before and after the degradation process of the BFO photoelectrode are summarized in table 1.

Table 1. Physical Properties of BFO photoelectrode before and after dye degradation process.

Concentration of BFO samples (mM)	Thickness (nm)		Structural properties		Bandgap (eV)	
	Before the degradation process	After the degradation process	Before the degradation process	After the degradation process	Before the degradation process	After the degradation process
4	75.8±5	73.3±5	Crystalline	Amorphous	2.01	1.95
6	92.3±5	88.8±5	Crystalline	Amorphous	2.13	2.01
8	101.4±5	98.7±5	Crystalline	Amorphous	2.19	2.09
10	127±5	120.6±5	Crystalline	Crystalline	2.33	2.25

Conclusion

Bismuth ferrite (BFO) thin films were synthesized via a simple spray pyrolysis method to achieve high-quality BFO material in thin film form at different precursor concentrations. All the BFO samples confirmed to be in single-phase with the rhombohedral crystal structure. The band-gap energies found to be between 2-2.33 eV, which are suitable for efficient photocatalytic degradation of Methylene blue (MB), Congo red (CR) and Ponceau-S (PS) dyes under visible-light irradiation. In particular, it was confirmed that BFO degrades MB dye as high as 74 % due to the reasons that the chromophore structure of the MB is easy to break using BFO film. The BFO sample deposited at 10 mM concentration is reused to check the stability of the material. After using BFO 10 mM sample three times, it still shows better hopes for further degradation. The enhanced photocatalytic activity of BFO can be attributed to the visible-light contribution and efficient charge separation in BFO. This degradation proves BFO can be used as efficient as well as a reusable electrode for the degradation of MB dye selectively. Our work puts insight into the understanding of the physical properties of the BFO electrode before and after the degradation process and hence, we believe that this work would be beneficial for other electrode studies, too.

Acknowledgment

Authors are grateful to the Department of Science and Technology (DST) for financial assistance through DST-INSPIRE Faculty research project [IFA 13-PH-61 dated 1 August 2013].

References

[1] Y. R. Smith, A. Kar and V. Subramanian, *Ind. Eng. Chem. Res.* **48** (2009) 10268-10276.

[2] T. Soltani, and M. H. Entezari, *Chem. Eng. Journal* **223** (2013) 145-154.

[3] T. Robinson, G. McMullan, R. Marchant and P. Nigam, *Biores. Technolol.***77** (2001) 247-255.

[4] D. H. Brown, H. R. Hitz and Schafer, *Chemosphere* **10 (**1981) 245-261.

[5] Y. Yang and L. Xu, *Am. Dystuff Rep*. **3** (1996) 27-34.

[6] A. G. S. Pradao, J. D. Torres, E. A. Faria and S. C. I. Dias, *Colloid Interface Sci.* **277 (**2004) 43-47.

[7] H. Kyung, J. Lee and W. Choi, *Environ. Sci. Tech.* **39 (**2005**)** 2376-2382.

[8] M. Muruganandham, N. Shobana and M. Swaminathan, *J. Mol. Cat. A:Chemical* **246** (2006) 154-161.

[9] R. M. Kumari, N. Thapa, N. Gupta, A. Kumar and S. Nimesh, *Adv. Nat. Sci: Nanosci. Nanotechnol.* 7 (2016) 045009.

[10] T. T. H. Tran, H. Kosslick, A. Schulz and Q. Nguyen, *Adv. Nat. Sci: Nanosci. Nanotechnol.* **8 (**2017) 015011.

[11] Van Cuong Nguyen, *Adv. Nat. Sci: Nanosci. Nanotechnol.* **5 (**2014) 035014.

[12] R. Chauhan, A. Kumar and R. P. Chaudhary, *J. Lumin* **145** (2014) 6-12.

[13] H. Lv, X. Shen, Z. Ji, D. Qui, G. Zau and Bi, *Appl. Surf. Sci.* **284** (2013) 308-314.

[14] Xu Chen, G. P. Rangaih and X. S. Zhao, *Ind. Eng. Chem. Res.* **53 (38)** (2014) 14641–14649.

[15] Z. Xiong, H. Dou, J. Pan, C. Xu and X. S. Zhao, *Cryst. Eng. Comm.* **12** (2010) 3455-3457.

[16] N. Xu, Z. Shi, Y. Fan, J. Dong, J. Shi and Z. M. Hu, *Ind. Eng. Chem. Res.* **38** (1999) 373-379.

[17] E. Repo, S. Rengaraj, S. Pulkka, E. Castangnoli, S. Suihkonen, M. Sopanen and M. Sillanpää, *Separation and Purification Technology* **120** (2013) 206–214.

[18] Z. Khan, T. R. ChetiaR, A. K. Vardhaman, C. V. Sastri and M. Qureshi, *RSC Adv.* **2 (**2012) 12122-12128.

[19] B. Pan, Y. Xie, S. Zhang, L. Lv, and W. Zhang, *ACS Appl. Mater. Interfaces* **4 (8)** (2012) 3938–3943.

[20] D. A. Shende, Y. N. Rane, M. G. Raghuwanshi, N. M. Gosavi, S. R. Gosavi, and N. G. Deshpande, *Optik* **161** (2018) 284-292.

[21] T. Choi, S. Lee, Y. J. Choi, V. Kiryukhin and S. W. Cheong, *Science* **324 (**2009) 63.

[22] D. W. Cao, Z. J. Wang, Nasori, L. Y. Wen, Y. Mi and Y. Lei, Angew. *Chem. Int. Ed.* **53** (2014) 11027.

[23] F. Gao, Y. Yuan, K. F. Wang, X. Y. Chen, F. Chen, J. M. Liu and Z. F. Ren, *Appl. Phys. Lett* **89** (2006) 102506.

[24] T. Gao, Z. Chen, Q. Huang, F. Niu, X. Huang, L. Qin and Y. Huang, *Rev. Adv. Mater. Sci.***40** (2015) 97-109.

[25] J. Wang, J. B. Neaton, H. Zheng, V. Nagarajan, S. B. Ogale, B. Liu, D. Viehland, V. Vaithyanathan, D. G. Schlom, U. V. Waghmare, N. A. Spaldin, K. M. Rabe, M. Wuttig, R. Ramesh, *Science New Series* **299** (2003) 1719-1722.

[26] V. A. Reddy, G. D. Verma and R. Nath, *AIP Advances* **1 (**2011) 042140.

[27] J. Deng, S. Banerjee, S. K. Mohapatra, Y. R. Smith, and M. Misra, *J. Fundamentals of Renewable Energy and Appls* **1 (**2011) R101204.

[28] T. Soltani, and M. H. Entezari, *Ultrasonics Sonochemistry* **20** (2013) 1245–1253.

[29] X. Y. Chen, T. Yu, F. Gao, H. T. Zhang, L. F. Liu, Y. M. Wang, Z. S. Li, and Z. G. Zou, *Appl. Phys. Lett.* **91** (2007) 022114.

[30] S. Y. Yang, L.W. Martin, S. J. Byrnes, T. E. Conry, S. R. Basu, D. Paran, *Appl Phys Lett* **95** (2009) 062909.

[31] S. Y. Yang, J. Seidel, S. J. Byrnes, P. Shafer, C. H. Yang, M. D. Rossell, *Nature Nanotechnology* **5** (2010) 143–147.

[32] P. Sathish, K. Ravichandran, B. Sakthivel and A. Panneerselvam, *Acta Metallurgica* Sinica, **28** (2015) 1407-1413.

[33] J. I. Langford and A. J. C. Wilson, *J. Appl. Cryst.* **11** (1978) 102-113.

[34] A. V. Moholkar, S. M. Pawar, K. Y. Rajpure and C. H. Bhosale Mater. Letts. **61** (2007) 3030-3036.

[35] R. J. Deokate, S. M. Pawar, A. V. Moholkar, V. S. Sawant, C. A. Pawar, C. H. Bhosale, and K. Y. Rajpure, Appl. Surf. Sci., **254** (2008) 2187-2195.

[36] R. N. Wenzel, J. Phys. Chem. **53** (1949) 1466–1467.

[37] A. B. D. Cassie and S. Baxter, Trans. Faraday Soc. **40** (1944) 546–551.

[38] Z. Yoshimitsu, A. Nakajima, T. Watanabe, and K. Hashimoto, Langmuir **18** (2002) 5818–5822.

[39] C. Ishino, K. Okumura, and D. Quéré, Europhys. Lett. **68** (2004) 419-425.

[40] T. Soltani, and M. H. Entezari, *J. Mol. Catal. A Chem* **377** (2013) 197-203.

[41] U. I. Gaya, and A. H. Abdullah, *J. Photoch. Photobio. C.* **9 (1)** (2008) 1-12.

[42] A. A. Telke, S. M. Joshi, S. U. Jadhav, D. P. Tamboli, S. P. Govindwar, *Biodegradation* **21** (2010) 283-296.

[43] A. Houas, H. Lachheb, M. Ksibi, E. Elaloui, C. Guillard, and J. M. Hermann, *Appl. Cata. B: Environ.* **31** (2001) 145-157.

[44] T. Zhang and Z-R Nan, *Desalination and Water Treatment* **57 (**2014) 4633-4640.

[45] A. Giwa, P. O. Nkeonye, K.A. Bello, K. A. Kolawole, *J. Environ. Protection* **3 (**2012) 1063-1069.